

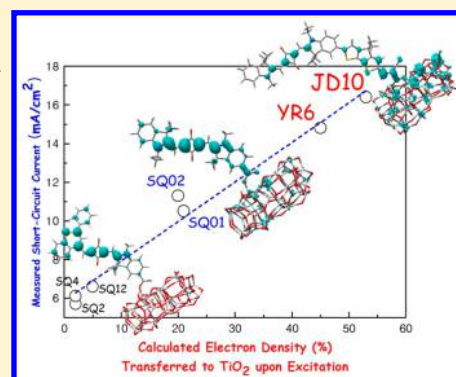
Electron Transfer of Squaraine-Derived Dyes Adsorbed on TiO_2 Clusters in Dye-Sensitized Solar Cells: A Density Functional Theory Investigation

Hui-Hsu Gavin Tsai,* Chun-Jui Tan, and Wen-Hsin Tseng

Department of Chemistry National Central University, Jhong-Li City, Tao-Yuan County 32001, Taiwan

S Supporting Information

ABSTRACT: Because the intense absorptions of squaraine (SQ) dyes in the red/near-infrared spectral regions closely match the spectral response of sunlight, SQ dyes have great potential for use in dye-sensitized solar cells (DSCs). In this study, we employed density functional theory (DFT) and time-dependent DFT to investigate the structural, optical, and electron transfer properties of seven recently reported SQ-derived dyes adsorbed on a $(\text{TiO}_2)_{38}$ cluster having an anatase (101) surface, as a model for corresponding DSCs. In particular, we calculated the proportions of the electron densities in the dye– $(\text{TiO}_2)_{38}$ systems that were transferred to the TiO_2 moieties upon excitation, allowing us to investigate their electron injection mechanisms. We found that the dye– $(\text{TiO}_2)_{38}$ systems followed different direct and indirect mechanisms of electron injection to TiO_2 depending on the localization of the excited state electron density and the driving force for excited-state electron injection. JD10 and YR6 owning two intense absorption bands, which have significant proportions of electron density delocalized into the TiO_2 moiety upon excitation and have driving forces for excited-state electron injection, followed direct electron injection mechanisms to TiO_2 . These results are compatible with their higher experimentally observed short-circuit currents (J_{sc}) than those of the SQ dyes. In contrast, SQ12, SQ2, and SQ4 followed the indirect electron injection mechanism due to their negligible proportion of electron density injected into TiO_2 ; in addition, SQ2 and SQ4 do not provide driving force for electron injection. SQ12, SQ2, and SQ4 dyes had lower experimentally observed J_{sc} values than those of the other SQ dyes. The calculated probabilities of electron density being delocalized into TiO_2 and driving force for excited-state electron injection from these studied SQ dyes are compatible with their experimentally observed J_{sc} values. This study provides insight into the electron injection mechanisms of SQ-derived dyes adsorbed on TiO_2 upon photoexcitation. Furthermore, our calculations and findings give clues for designing new SQ-derived sensitizers for DSC applications.



■ INTRODUCTION

Environmental problems related to nonrenewable energy, such as petroleum and coal, have become matters of grave concern; in addition, these resources are becoming expensive as supplies are decreasing and demand is increasing. Therefore, the development of clean, renewable energy has become an urgent priority, with solar energy being one of the most promising. In particular, dye-sensitized solar cells (DSSCs or DSCs) have attracted considerable interest since their invention by O'Regan and Grätzel,^{1,2} in particular because of their low manufacturing cost. In addition, DSCs open up the possibility of designing solar cells having flexible shapes, various colors, and transparency. DSCs harvest solar energy through dyes adsorbed on the semiconductor titanium dioxide (TiO_2) strongly absorbing solar radiation. The electrons of the photoexcited dye are injected into the conduction band of the semiconductor anode prior to charge recombination. The oxidized dye is restored to its reduced state by a redox couple in the electrolyte solution (commonly I^-/I_3^-). The injected electron on the semiconductor electrode generates a photocurrent passing through

an external load to the counter electrode, where the I^- ion is restored through reduction of I_3^- , completing the circuit.

In functioning DSCs, the dye sensitizer plays two critical roles: the absorption of sunlight and the injection of electrons into the semiconductor. To achieve high power conversion efficiencies (PCEs), dye sensitizers must absorb incident light well—in particular, the strong solar radiation in the range from 400 to 900 nm. It is believed that dyes that absorb at wavelengths extending into the far-red/near-infrared (IR) may improve cell efficiency because of their good spectral match with solar emission.^{3–5} To achieve sufficient light absorption for high PCEs, dyes with higher molar absorption coefficients (ϵ) are naturally of great interest.^{6,7} Furthermore, energy alignment of the excited state of the dye sensitizer with the conduction band of the semiconductor also requires fine-tuning to optimize the efficiency of electron injection.^{8,9} One of the

Received: August 8, 2014

Revised: January 16, 2015

Published: February 6, 2015



keys to realizing the potential of dye sensitization in DSC applications is to optimize these various parameters.

Several classes of dye sensitizers for DSCs have been studied, including ruthenium (Ru) complexes, porphyrin, squaraine (SQ) derivatives, and other metal-free organic dyes. Heteroleptic Ru complexes are highly effective dye sensitizers. Several Ru dyes, including N719¹⁰ and CYC-B11,¹¹ have yielded DSCs displaying promising PCEs of greater than 11%. Ruthenium dyes comprise a central Ru(II) ion with ancillary ligands and at least one anchoring group; they absorb broadly in the visible region, mainly because of metal-to-ligand charge transfer (MLCT), with molar absorption coefficients of approximately $30\,000\text{ M}^{-1}\text{ cm}^{-1}$. Insufficient light-harvesting ability in the near-IR region of the solar spectrum is one of the shortcomings of Ru complexes.^{4,12} Some attempts have been made to tune the absorption of the MLCT band to a longer wavelength and increase the absorbance by modifying the ancillary bipyridyl ligand with various substituents.^{6,7} Using such an approach, the absorption maximum (λ_{max}) of the low-energy MLCT band was recently red-shifted to 630 nm, but the value of ϵ remained moderate ($6430\text{ M}^{-1}\text{ cm}^{-1}$).¹³ Despite these advances, environmental issues and the rarity and high cost of Ru have encouraged scientists to explore cheaper and safer sensitizers as alternatives. Among the wide range of possible dyes, porphyrin-based dyes are interesting because of their broad absorptions and relatively intense spectral responses in the near-IR region. Porphyrins have rigid molecular structures and possess good chemical, photo-, and thermal stability. In 2011, an ortho-substituted push-pull zinc porphyrin (YD2-o-C8) cosensitized DSC, in combination with a Co-based electrolyte, achieved a new PCE record of 12.3%.¹⁴ The dye YD2-o-C8 has an intense Soret band at 448 nm ($\epsilon = 212\,000\text{ M}^{-1}\text{ cm}^{-1}$) and a weaker Q-band at longer wavelength ($\lambda_{\text{max}} = 645\text{ nm}$) with a corresponding value of ϵ of up to $31\,200\text{ M}^{-1}\text{ cm}^{-1}$. Obviously, the absorbance of the Soret band of YD2-o-C8 is much stronger than that of the MLCT band of N719, while the absorbance of the Q-band of YD2-o-C8 is similar to that of the MLCT band of N719. Recently, sensitization using a zinc-porphyrin-based donor- π -acceptor (D- π -A) dye, while employing Co-based electrolytes, has led to a new efficiency record of 13%.¹⁵ Metal-free organic dyes have also received attention because of their relatively high molar absorption coefficients, facile structural modifications, tunable spectral properties, and simple syntheses. One advantage of metal-free organic dyes is that they are not associated with concerns about limited resources. Recently, a quinoxaline-based D- π -A dye, YA422, was reported by Grätzel and colleagues to yield a device having a PCE of 10.65%,¹⁶ comparable with the PCEs of Ru- and porphyrin-based dyes. Unlike the narrow absorption ranges of most organic dyes, YA422 absorbs light over the entire visible range; its lowest-energy absorption peak is located at 534 nm ($\epsilon = 27\,400\text{ M}^{-1}\text{ cm}^{-1}$) and its highest-energy absorption peak is located at 388 nm ($\epsilon = 53\,000\text{ M}^{-1}\text{ cm}^{-1}$).

The absorptions of squaraine (SQ) dyes, usually in the range from 600 to 800 nm, are more red-shifted than those of most organic dyes and Ru complexes. In particular, the absorption coefficients of SQ-derived dyes are much larger than those of most organic dyes, Ru complexes, and porphyrin-derived dyes, which provide devices with high PCEs, as mentioned above. SQ-derived dyes have promising applications in DSCs as well as in organic photovoltaic cells.^{17,18} Symmetrical SQ dyes based on D-A-D frameworks and having carboxyethyl anchoring groups attached to the N atom of the indoline ring have been

applied in DSCs since 2005.^{19,20} Theoretical investigations have revealed that electrons flow toward the center of such symmetrical SQ dyes upon photoexcitation.²⁰ Several studies have emphasized that unidirectional flow of electron density is favorable for charge separation and ready electron injection.^{21–23} Moreover, earlier research has suggested that anchoring groups should be as close as possible to the chromophore to enhance the incident photon-to-current efficiency (IPCE) performance.²⁴ In 2007, Grätzel and colleagues reported SQ01, an unsymmetrical SQ dye based on a D- π -spacer-A framework and featuring a carboxylic acid anchor attached directly to the benzene ring of the indoline unit. Although SQ01 has a value of λ_{max} of 636 nm with a high value of ϵ of $158\,500\text{ M}^{-1}\text{ cm}^{-1}$, its cell exhibited a PCE of only 4.5%. HSQ1, a cis-configured squaraine dye, has provided cosensitized DSCs exhibiting energy-conversion efficiencies of up to 8.14%. A comprehensible mechanism has been suggested for the influence of the configuration of HSQ1 on TiO₂ on the performance of the cosensitized DSC devices.²⁵ To improve the efficiency of SQ sensitizers, cyanoacrylic acid has been adopted as an anchor to further create directionality of electron transfer.²⁶ Using this approach, the dye JD10, which has a value of λ_{max} of 680 nm with a value of ϵ of $230\,000\text{ M}^{-1}\text{ cm}^{-1}$, has provided a device exhibiting the highest PCE (7.3%) among those based on all known SQ-derived dyes.⁷ Their extremely high absorbances and red-shifted absorption regions make SQ-derived dyes ideal candidates for practical use in DSCs. Recently, efforts have been devoted to designing various unsymmetrical SQ dyes for DSC applications. Enhancing the performance of SQ dye-based solar cells has been attempted by improving the directionality of electrons following photoexcitation (e.g., by extending the conjugation length or replacing functional groups).^{7,12,21,27–30} Nevertheless, these SQ dyes still provide lower device efficiencies than those of devices incorporating Ru complex dyes, porphyrin-based dyes, or other classes of organic dyes.

SQ dyes have good spectral matches with solar radiation and large extinction coefficients; however, SQ-based DSCs do not have high PCEs. The low to moderate PCEs of SQ dye-based devices may be due to severe dye aggregation and intermolecular quenching.^{12,23,27,31} Moreover, the efficiency of electron injection of SQ-based dyes to the semiconductor might also be a factor affecting the PCEs of SQ-based dyes in DSC applications. Many theoretical calculations have been performed to study the electron transfer of dye sensitizers. Time-dependent density functional theory (TD-DFT) is commonly employed to qualitatively investigate the tendency of electron transfer of free dye sensitizers in solution upon photoexcitation by visualizing the electron density of the LUMO on the anchoring moiety.^{32–34} Hsu and co-workers calculated the differences in Mulliken charges of free dye molecules in the excited states and ground states projected from the TD-DFT results. The Mulliken charge difference between the various segments (in particular, the donor and acceptor units) allows estimation of the extent of charge separation upon photoexcitation.³⁵ Using electron density difference maps (EDDMs) derived from the transition electron density of dyes before and after excitation, our group has calculated the electronic transitions of various segments of free dyes to estimate the probability of electron transfer from one specific segment to another in a more quantitative manner.³⁶ Recently, theoretical calculations of dye sensitizers have advanced from free dyes to dye/TiO₂ systems. De Angelis

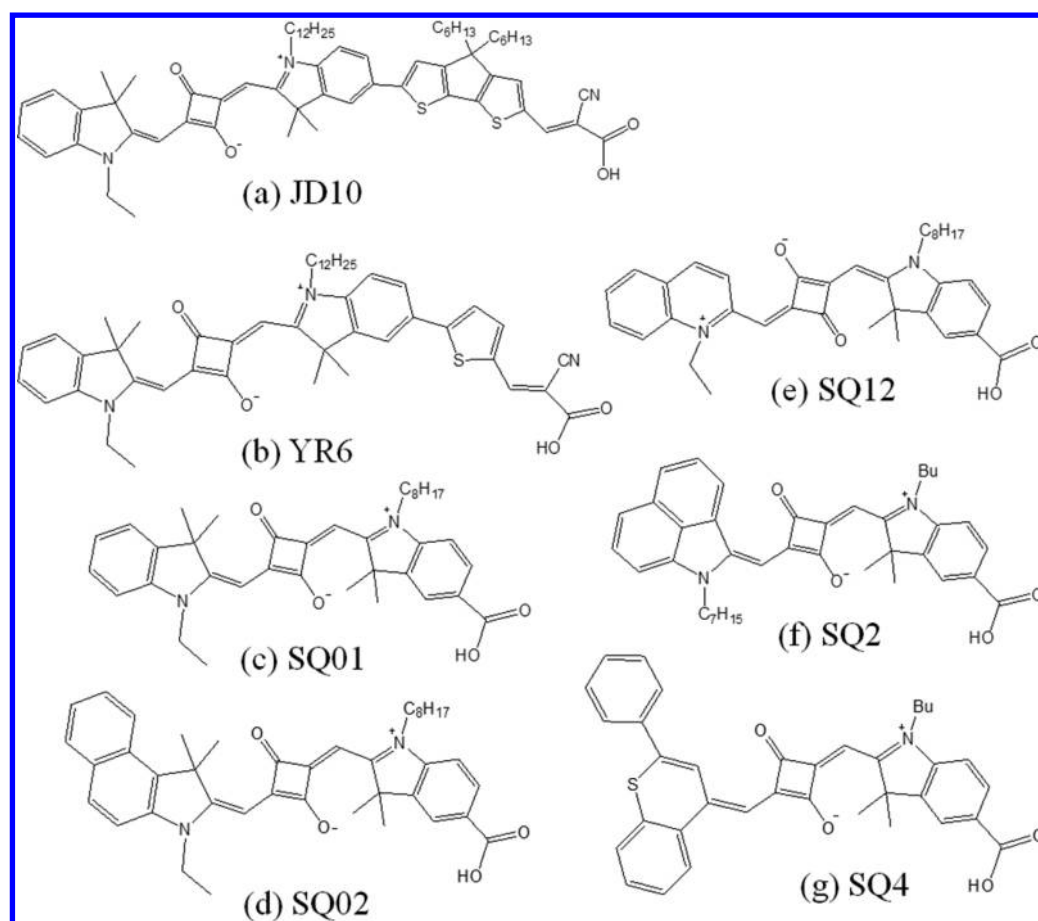


Figure 1. Chemical structures of the seven studied SQ dye sensitizers: (a) JD10, (b) YR6, (c) SQ01, (d) SQ02, (e) SQ12, (f) SQ2, and (g) SQ4.

and colleagues investigated the electron injection mechanisms of SQ/TiO₂ systems by analyzing the TD-DFT optical spectra and the changes in charge response before and after adsorption of the dyes. They concluded that both direct and indirect mechanisms are active for electron injection from SQ dyes to TiO₂, with the indirect injection mechanism dominating in this system.³⁷ Cao and colleagues compared the partial charge densities at the gamma (G) points of the bands of dye–TiO₂ systems with the molecular orbitals of the free dyes to rationalize the direct and indirect electron injection mechanisms.^{38,39} Our group has calculated the UV–vis spectra of some W-series dyes adsorbed directly on a (TiO₂)₃₈ cluster and analyzed their EDDMs upon photoexcitation. We correlated the probability of the electron density of W-dyes transferring to (TiO₂)₃₈ clusters with the experimentally measured short-circuit currents.⁴⁰ Troisi and colleagues developed a theoretical method to calculate the electron injection rate by assuming the same coupling matrix between different dyes and the TiO₂ interface, allowing the electron injection rate to be predicted rapidly using information about the free molecule.⁸

In this study, we employed DFT and TD-DFT to investigate the structural, optical, and electron transfer properties of seven SQ-based dyes in solution and adsorbed on a TiO₂ cluster having an anatase (101) surface. Figure 1 displays the chemical structures of the dyes we have investigated: JD10,⁷ YR6,²⁶ SQ01,²³ SQ02,²⁷ SQ12,³⁰ SQ2,⁴¹ and SQ4.⁴¹ We determined the proportion of direct electron transfer from these dyes to the TiO₂ cluster upon photoexcitation in terms of EDDM analysis and their lowest driving forces for excited-state electron

injections. Our results reveal that the dye–(TiO₂)₃₈ systems follow different direct and indirect mechanisms of electron injection to TiO₂ depending on the localization of the excited state electron density and the driving force for excited-state electron injection. We have found that the calculated proportions of electron density being delocalized into TiO₂ upon excitation from these studied SQ dyes are correlated with their experimentally observed J_{sc} values.

■ COMPUTATIONAL METHODS

The ground state molecular geometries of the studied free molecules (Figure 1) in EtOH solution were optimized using Becke's three-parameter exchange functional,⁴² the Lee–Yang–Parr gradient-corrected correlation functional,⁴³ and the 6-31G(d,p) basis set,⁴⁴ as implemented in the program Gaussian 09.⁴⁵ The molecules were optimized at their protonated and deprotonated states. All the long alkyl chains were replaced with methyl groups to save computational resources. The conductor-like polarizable continuum model (C-PCM)⁴⁶ was used to account for the EtOH solvation effect. The UV–vis spectra of all the free molecules in EtOH were calculated using TD-DFT. To study the charge transfer excitation properties, the coulomb-attenuating method (CAM)⁴⁷ was applied [at the CAM-B3LYP/6-31G(d,p) theoretical level] to calculate the UV–vis spectra.

To model the experimental properties of dye molecules adsorbed on TiO₂ thin films, dyes adsorbed on (TiO₂)₃₈ clusters were studied. The dye adsorbed on the anatase (101) surface of the (TiO₂)₃₈ supercluster⁴⁸ in a bidentate manner

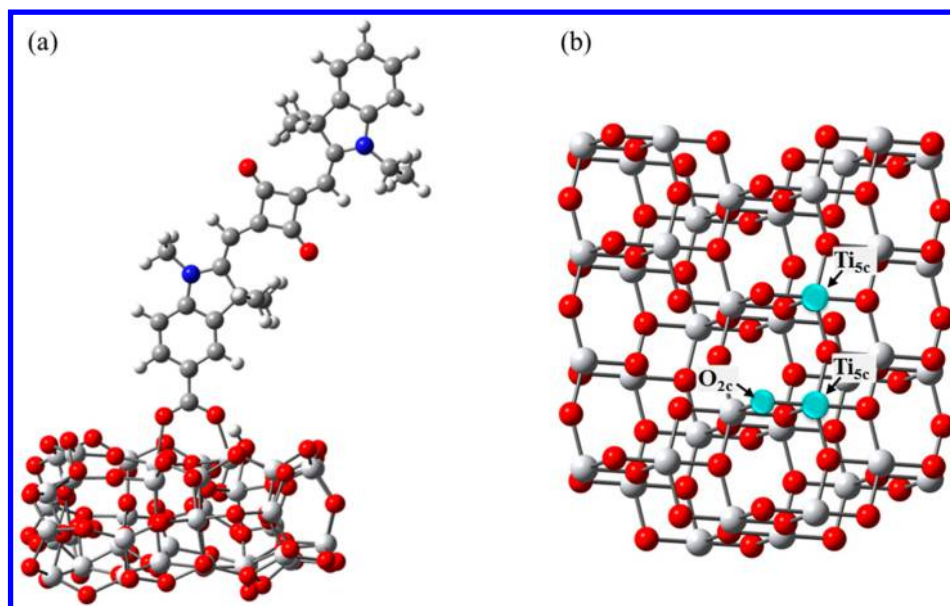


Figure 2. Dye adsorbed on a $(\text{TiO}_2)_{38}$ cluster. (a) Side view of SQ01 adsorbed on five-coordinated Ti atoms of a $(\text{TiO}_2)_{38}$ cluster; (b) top view of a $(\text{TiO}_2)_{38}$ cluster with an anatase (101) surface highlighting two five-coordinated Ti atoms and the protonated O atom.

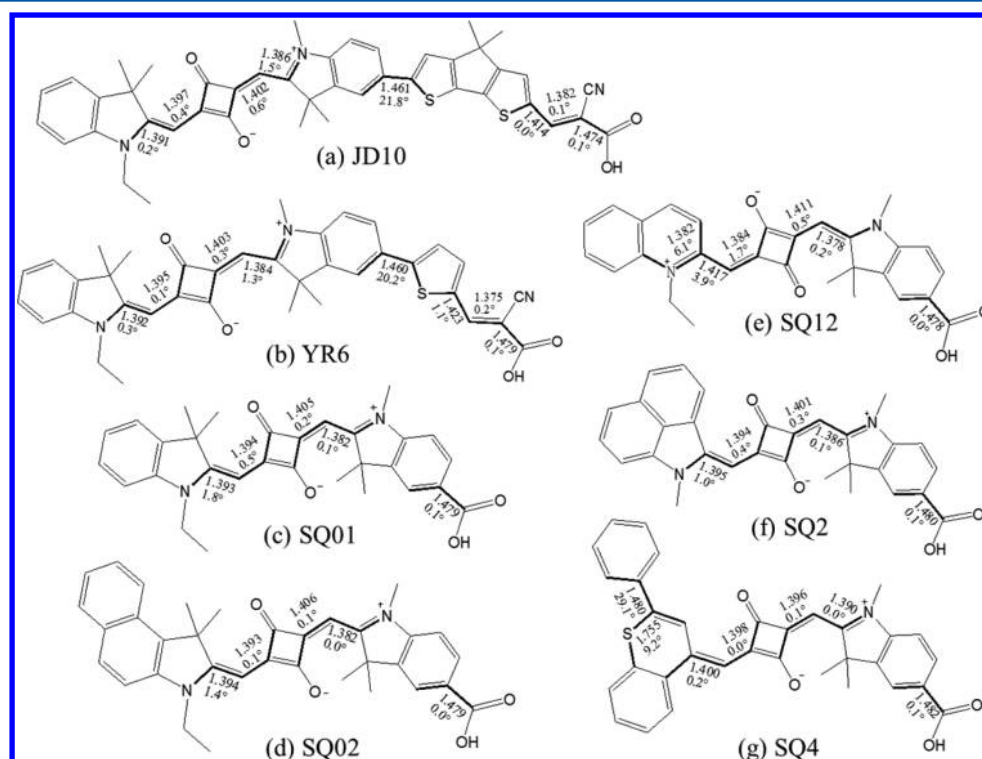


Figure 3. Selected molecular geometries for the seven studied SQ dyes at their protonated states: (a) JD10, (b) YR6, (c) SQ01, (d) SQ02, (e) SQ12, (f) SQ2, and (g) SQ4. The bond lengths (Å) are labeled around their corresponding bonds (units are not shown for clarity). The dihedral angles (deg) are labeled around their corresponding central bonds; their four consecutive bonds are highlighted in bold.

with one proton transferred to a nearby surface oxygen atom (O_{2c}), such that the two O atoms of the carboxylic acid are bound to the two neighboring five-coordinated Ti atoms (Ti_{5c}) on the TiO_2 surface (see Figure 2). Previous calculations have shown that for the organic dyes bearing a carboxylic acid as the anchoring group preferred this adsorption mode.^{49,50} This model system was chosen as a compromise between computational cost and the stated purpose of predicting the properties of dyes on TiO_2 thin films. The ground state molecular

geometries of the dye- $(\text{TiO}_2)_{38}$ complexes were optimized using the DMol3 software package.^{51,52} Perdew–Burke–Ernzerhof (PBE) parametrization of the generalized gradient approximation (GGA),⁵³ in conjunction with the double numerical basis sets with polarization (DNP), was adopted in the geometry optimization.⁵⁴ The quality of Gaussian 09 default optimization and all-electron core treatment was used in geometry optimization of the dye- $(\text{TiO}_2)_{38}$ systems. Finally, the optimized structures of all the studied dye- $(\text{TiO}_2)_{38}$

Table 1. Experimental (exp) and Computational Electronic Absorptions of Studied SQ Dyes in EtOH at Their Protonated States and Deprotonated States and Adsorbed on TiO₂

dyes	in EtOH								adsorbed on TiO ₂		
	exp		calculation (protonated state)			calculation (deprotonated state)			exp	calculation	
	ϵ_{max} (M ⁻¹ cm ⁻¹)	λ_{max} (nm)	f^b	λ_{max} (nm)	deviation from exp	f^b	λ_{max} (nm)	deviation from exp	λ_{max} (nm)	λ_{max} (nm)	deviation from exp
JD10 ⁷	250 000	672	2.57	590	−82	2.32	581	−99	670	595	−75
	38 000	474	0.88	472	−2	1.03	427	−47	460	488	28
YR6 ²⁶	279 000	659	2.23	586	−73	2.09	576	−83	663	591	−72
	17 000	420	0.51	423	+3	0.76	371	−49	425	440	15
SQ01 ²³	158 500	636	1.81	563	−73	1.79	561	−75	651	571	−80
SQ02 ²⁷	319 000 ^a	662 ^a	1.84	571	−91	1.80	572	−90	—	580	—
SQ12 ³⁰	120 000	656	1.89	583	−73	1.90	594	−62	664	592	−73
SQ2 ⁴¹	89 125	782	1.67	671	−111	1.67	665	−117	720	681	−39
SQ4 ⁴¹	85 144	785	1.67	680	−105	1.65	655	−130	706	700	−6

^aIn DMF. ^bOscillator strength.

complexes were used to calculate their UV–vis spectra, using the CAM-B3LYP/6-31G(d,p) method with Gaussian 09⁴⁵ in water (modeled by C-PCM). The EDDMs corresponding to the electronic transitions that visually revealed the changes in electron density before and after transitions were generated using GaussSum (v. 2.2.6).⁵⁵

RESULTS AND DISCUSSION

In this study, we performed DFT and TD-DFT calculations for seven recently published unsymmetrical SQ-derived dyes: JD10,⁷ YR6,²⁶ SQ01,²³ SQ02,²⁷ SQ12,³⁰ SQ2,⁴¹ and SQ4⁴¹ (Figure 1). These SQ dyes have been used to prepare DSCs and their photoproperties have been reported. These dyes share an SQ-indoline moiety, but differ in the nature of their donors, spacers, and anchors. SQ01 is a simple squaraine dye comprising an indoline unit as the electron donating group connected to the squaric moiety; it uses a carboxylic acid as the anchoring group linked to the π -system. SQ01 was the first squaraine sensitizer to provide a device exhibiting a PCE of up to 4.5%, a result that has been attributed mainly to the directionality of electron transfer and the inhibition of dye aggregation.²³

Similar to SQ01, YR6 and JD10 also feature an indoline unit as the electron-donating group, but in contrast to SQ01 they incorporate a more-extended π -conjugated moiety. YR6²⁶ was developed by Shi et al.; it produced a functioning device having a reported efficiency of 6.74% and a short circuit current (J_{sc}) of 14.8 mA cm⁻². YR6 incorporates one more thiophene ring as a spacer and has a cyanoacrylic acid moiety as an electron acceptor. JD10 has a structure similar to that of YR6, with a di-*n*-hexyl-substituted cyclopentadithiophene (CPDT) group replacing the thiophene group in YR6. JD10⁷ was developed by Dualeh et al.; it produced a functioning device with a reported efficiency of 7.30% and a value of J_{sc} of 16.4 mA cm⁻².

Each of SQ12, SQ2, and SQ4 has a molecular framework similar to that of SQ01, but with a different electron donating group: quinolone, benz[*c,d*]indolium, benzo[*e*]-indolium, and benzo-1-thiopyrylium, respectively. These molecules have a carboxylic acid unit as their anchoring group. A device incorporating SQ02⁴¹ had a reported efficiency of 5.4% and a value of J_{sc} of 11.3 mA cm⁻². Devices based on SQ12, SQ2, and SQ4 had poor efficiencies of 2.29, 1.10, and 1.23%, respectively, with low values of J_{sc} of 6.6, 5.7, and 6.1 mA cm⁻², respectively. Table S1 (see supporting materials) summarizes the reported photovoltaic parameters of these


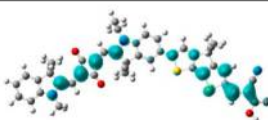

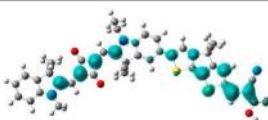
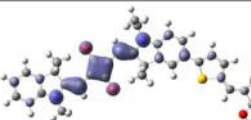
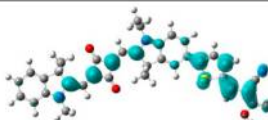
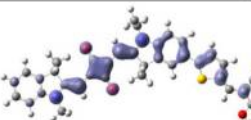
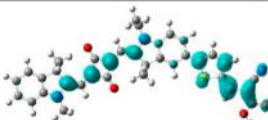
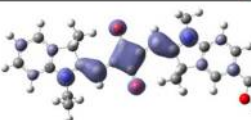

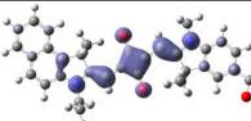

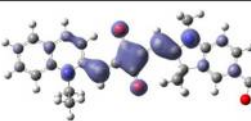
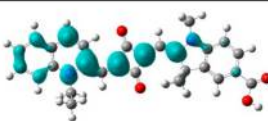
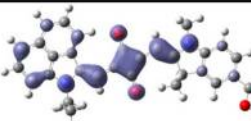

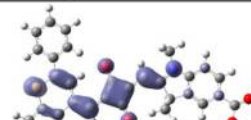
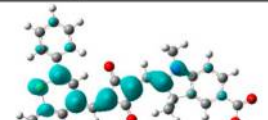
studied SQ-based DSSCs. Because these SQ-dyes have different donors, spacers, and anchor groups, we could investigate how changes in these structural characteristics affected their optical and electron transfer properties. Moreover, devices based on these dyes have values of J_{sc} ranging from high to low, allowing us to examine how the calculated electron transfer properties correlated with their values of J_{sc} .

Molecular Geometries. The ground state molecular geometries of the seven SQ dyes at their protonated states in EtOH were optimized at the B3LYP/6-31G(d,p) level with the C-PCM solvent model. Figure 3 displays selected structural parameters of these molecules. These structural parameters are mainly the bond lengths and dihedral angles of the two adjacent rigid aromatic rings, which are most sensitive to the chemical environments; therefore, they will influence each dye molecule's degree of π -conjugation and, thus, affect their absorption spectra. For each studied system, the SQ ring was planar. Paterson et al. performed a thorough theoretical investigation of SQ chromophores;⁵⁶ the optimized structure of squaric acid in the ground state was observed to be bent. In our calculations at the B3LYP/6-31G(d,p) level, the dihedral angle of the central four-membered ring of squaric acid in the gas phase was approximately 29° (detailed data not shown). The SQ chromophore becomes planar after the hydrogen atoms on both sides are replaced by an electron donor and acceptor, which stabilize the resonance planar structures in the ground state.⁵⁷

SQ01, SQ02, and SQ2 are nearly planar throughout their entire molecules, having all dihedral angles of the backbone and anchor close to 0°. The molecular frameworks of SQ12 and SQ4 are nearly planar, except for the two dihedral angles labeled in Figure 3. The C–C bond lengths in the central SQ rings are approximately 1.48 Å; the bond lengths between the aromatic rings in these dyes are in the range 1.382–1.417 Å—greater than a C=C double bond (*ca.* 1.34 Å), but shorter than a C–C single bond (*ca.* 1.54 Å); these features are consistent with electron delocalization between adjacent moieties, and indicate that the squaric rings were conjugated well in the molecules.

Interestingly, dyes with extended moieties in the π -bridge—for example, JD10 and YR6—featured twisting of their indoline ring and additional aromatic ring (CPDT in JD10; thiophene in YR6). The dihedral angles in JD10 and YR6, defined as the planarity between the indoline ring and the additional aromatic ring, were 21.8 and 20.2°, respectively, with corresponding

Table 2. Orbital Contributions and EDDMs of the studied dyes upon photo-excitation at their protonated state in EtOH

Dye	λ_{\max} (nm) & f^a	Transitions ^b	EDDM (where the electron density is coming from)	EDDM (where the electron density is going)
JD10	$\lambda_{\max} = 590$ $f = 2.57$	H \rightarrow L (49%) H \rightarrow L+1 (41%) H-1 \rightarrow L+1 (5%)		
	$\lambda_{\max} = 472$ $f = 0.88$	H-1 \rightarrow L (53%) H \rightarrow L+1 (29%) H-1 \rightarrow L+1 (6%) H \rightarrow L (6%)		
YR6	$\lambda_{\max} = 586$ $f = 2.23$	H \rightarrow L (69%) H \rightarrow L+1 (25%)		
	$\lambda_{\max} = 423$ $f = 0.51$	H \rightarrow L+1 (54%) H-1 \rightarrow L (23%) H \rightarrow L (12%) H-1 \rightarrow L+1 (7%)		
SQ01	$\lambda_{\max} = 563$ $f = 1.81$	H \rightarrow L (97%)		
SQ02	$\lambda_{\max} = 571$ $f = 1.84$	H \rightarrow L (97%)		
SQ12	$\lambda_{\max} = 583$ $f = 1.89$	H \rightarrow L (96%)		
SQ2	$\lambda_{\max} = 671$ $f = 1.67$	H \rightarrow L (97%)		
SQ4	$\lambda_{\max} = 680$ $f = 1.67$	H \rightarrow L (98%)		

^aOscillator strength. ^bH = HOMO; L = LUMO. The transitions with contribution larger than 5% are shown.

central bond lengths of 1.461 and 1.460 Å, respectively. These two bond lengths are significantly longer than others connecting two aromatic rings. Thus, introduction of additional rings between the indoline and anchoring group did not fully extend the conjugation length of the dye molecules. On the other hand, the CPDT group in JD10 and the thiophene group in YR6 are nearly coplanar with their anchoring groups.

The molecular geometries of dyes influence their photo-physical and photochemical properties. Planar SQ dyes are known to form aggregates, leading to dissipative intermolecular charge transfer and also rapid charge recombination, resulting in decreased DSC performance.^{3,58} A relationship exists between the structural planarity of a dye and its aggregation.^{58–60} In 2007, Choi et al. introduced a nonplanar

dimethylfluorenyl unit to novel organic dyes to prevent their aggregation through molecular stacking.⁶⁰ Recently, Hua et al. reported that phenothiazine-based dyes having a nonplanar butterfly conformation suppressed molecular aggregation and decreased the rate of internal charge recombination, thereby improving cell efficiency.⁶¹ The efficiencies of cells incorporating JD10 and YR6 are higher than those of devices based on our other studied systems. We found that JD10 and YR6 are nonplanar, potentially decreasing their degrees of aggregation and, thereby, leading to better cell performance.

Absorption Spectra of SQ Dyes. Table 1 lists optical data obtained from both experimental observations and TD-DFT calculations [performed using the CAM-B3LYP functional with the 6-31G(d,p) basis set] of the SQ dyes in EtOH solutions at

Table 3. Electron Density of SQ Dyes at their Protonated States in EtOH Solution before (Where the Electron Density Is Coming from) and after (Where the Electron Density Is Going) Transition

dye	λ_{abs} /oscillator strength		change	percent contribution (%)				
				donor ^a	SQ	indoline	R ^b	anchor ^c
JD10	#1	590 nm $f = 2.57$	before	29	24	35	10	2
			after	15	19	16	29	21
			net	−14	−5	−19	+19	+19
	#2	472 nm $f = 0.88$	before	17	14	23	37	9
			after	13	17	16	31	23
			net	−4	+3	−7	−6	+14
YR6	#1	586 nm $f = 2.23$	before	31	27	37	4	1
			after	15	19	19	21	26
			net	−16	−8	−18	+17	+25
	#2	423 nm $f = 0.51$	before	26	21	36	11	6
			after	16	21	19	19	25
			net	−10	0	−17	+8	+19
SQ01		563 nm $f = 1.81$	before	33	29	37	−	1
			after	32	39	27	−	2
			net	−1	+10	−10	−	+1
SQ02		571 nm $f = 1.84$	before	36	28	35	−	1
			after	33	39	26	−	2
			net	−3	+11	−9	−	+1
SQ12		583 nm $f = 1.89$	before	29	30	40	−	1
			after	49	31	19	−	1
			net	+20	+1	−21	−	0
SQ2		671 nm $f = 1.67$	before	40	27	32	−	1
			after	49	29	21	−	1
			net	+9	+2	−11	−	0
SQ4		680 nm $f = 1.67$	before	43	27	29	−	1
			after	43	31	25	−	1
			net	0	+4	−4	−	0

^aQuinoline for SQ12, benz[*c,d*]indolium for SQ2, benzo-1-thiopyrylium for SQ4, and indoline ring for others. ^bCPDT for JD10 and thiophene for YR6. ^cCyanoacrylic acid for JD10 and YR6 and carboxylic acid for other dyes.

their protonated and deprotonated states. The calculated electronic excitation energies of dyes at their protonated states have smaller deviation from their corresponding experimental data than those calculated at deprotonated states. The trends in the calculated electronic absorptions of the free dye molecules in solution agree with the experimental observations; at the protonated state, the smallest deviation from the experimental value was a 2 nm blue-shift for the higher-energy band of JD10, while the largest deviation was a 111 nm blue-shift for SQ2. The average absolute deviation between the calculated absorption maxima for the free molecules in solution and those observed experimentally was 68 nm. The calculated excitation energies of the SQ dyes in EtOH solution are generally substantial blue-shifted in relative to their corresponding experimental data. These calculated errors are generally larger than those determined previously for organic dyes, such as W-dyes, which had absolute deviations within 10 nm for the free molecules.⁴⁰ In TD-DFT calculations, molecules having a diradical nature usually deviate to a greater extent from experimental observations.⁶² Moreover, the SQ dyes and EtOH may form hydrogen bonds, which are not well considered explicitly in the C-PCM solvent model. The dyes SQ01, SQ02, SQ12, SQ2, and SQ4, which have similar molecular frameworks, all featured a single strong absorption band in their experimental and computational absorption spectra. On the other hand, YR6 and JD10 provided two absorption bands, with the lower-energy band being more intense than the higher-energy band. For the higher-energy band, the calculated values

of λ_{max} of JD10 and YR6 at their protonated states were in excellent agreement with the experimental results, with absolute errors of only 2–3 nm.

In terms of the experimental absorption spectra, the values of λ_{max} of these studied SQ dyes did not correlate well with their π -conjugation lengths determined simply based on their chemical structures. For example, SQ2 and SQ02 have similar π -conjugation lengths, but distinct values of λ_{max} . SQ2 has a value of λ_{max} of 782 nm, while SQ02 has a value of 662 nm—a blue-shift of more than 120 nm relative to SQ2. Moreover, YR6 has a longer π -conjugation length than SQ02, yet YR6 and SQ02 have similar values of λ_{max} . SQ dyes are characterized by their intense absorptions in the far-red to near IR domain. The decrease in the highest occupied molecular orbital (HOMO)–LUMO gap could be ascribed to the increase in π -electron density of the molecular backbone, which leads to better conjugation, and also an increase in diradical character.⁵⁷ A positive correlation has been found between the diradical character and the absorption wavelength.⁶²

Table 2 lists the orbital contributions and EDDMs of the dyes of interest upon photoexcitation at their protonated state in EtOH. Electron density difference map (EDDM) illustrates the changes of electron density that occurs when a system changes its state. EDDM is obtained by subtracting the electron density before an electronic transition (e.g., ground state), from the electron density after (e.g., first excited state).⁶³ EDDM is useful to elucidate the electron migration intuitively upon photoexcitation.^{39,64,65} All of our studied SQ dyes share an

Table 4. Computational Electronic Absorptions and EDDMs of SQ Dyes Absorbed on $(\text{TiO}_2)_{38}$ Cluster

dye	λ_{abs}/f^a		transitions ^b	change	percent contribution (%)					
					donor ^c	SQ	indoline	R ^d	anchor ^e	$(\text{TiO}_2)_{38}$
JD10	#1	595 nm $f = 2.83$	H \rightarrow L (28%)	before	29	23	35	11	2	0
			H \rightarrow L + 9 (22%)	after	7	9	7	13	11	53
			H \rightarrow L + 8 (21%)	net	−22	−14	−28	+2	+9	+53
			H \rightarrow L+1 (6%)							
	#2	488 nm $f = 1.07$	H − 1 \rightarrow L (43%)	before	17	14	23	36	10	0
			H \rightarrow L + 9 (15%)	after	5	7	7	19	15	47
			H \rightarrow L + 8 (11%)							
			H − 1 \rightarrow L + 1 (8%)	net	−12	−7	−16	−17	+5	+47
			H \rightarrow L (7%)							
YR6	#1	591 nm $f = 2.38$	H \rightarrow L (51%)	before	32	26	36	4	2	0
			H \rightarrow L + 9 (9%)							
			H \rightarrow L + 10 (8%)	after	6	7	9	14	19	45
			H \rightarrow L + 4 (6%)							
			H \rightarrow L + 6 (5%)	net	−26	−19	−27	+10	+17	+45
	#2	440 nm $f = 0.67$	H \rightarrow L + 11 (5%)							
			H − 1 \rightarrow L (25%)	before	27	21	35	11	6	0
			H \rightarrow L (19%)							
			H \rightarrow L + 10 (11%)	after	5	7	8	12	17	51
			H \rightarrow L + 13 (10%)							
			H \rightarrow L + 9 (8%)	net	−22	−14	−27	+1	+11	+51
			H \rightarrow L + 11 (7%)							
SQ01		571 nm $f = 2.06$	H \rightarrow L + 2 (88%)	before	34	29	36	—	1	0
				after	24	30	22	—	3	21
				net	−10	+1	−14	—	+2	+21
SQ02		580 nm $f = 2.12$	H \rightarrow L + 2 (87%)	before	37	27	35	—	1	0
				after	25	30	22	—	3	20
				net	−12	+3	−13	—	+2	+20
SQ12		583 nm $f = 2.16$	H \rightarrow L (95%)	before	28	30	41	—	1	0
				after	46	30	18	—	2	5
				net	+18	0	−23	—	+1	+5
SQ2		681 nm $f = 1.85$	H \rightarrow L (97%)	before	41	26	32	—	1	0
				after	49	29	19	—	1	2
				net	+8	+3	−13	—	0	+2
SQ4		700 nm $f = 1.90$	H \rightarrow L (97%)	before	40	27	32	—	1	0
				after	47	29	21	—	1	2
				net	+7	+2	−11	—	0	+2

^aOscillator strength. ^bThe transitions with contribution larger than 5% are shown. ^cQuinoline for SQ12, benz[*c,d*]indolium for SQ2, benzo-1-thiopyrylium for SQ4 and indoline for others. ^dCPDT for JD10 and thiophene for YR6. ^eCyanoacrylic acid for JD10 and YR6; carboxylic acid for other dyes.

intense $\pi \rightarrow \pi^*$ absorption, where the electron density is transferred mainly from the HOMO to the LUMO (JD10 and YR6 have significant electron density transferred from HOMO to LUMO+1). Figure S1 (Supporting Information) displays the HOMO and LUMO of SQ01. The HOMO of SQ01 has no nodal plane in the squaric four-membered ring perpendicular to the molecular plane; there is one nodal plane perpendicular to the squaric four-membered ring. The other SQ dyes had similar features for their orbital contributions from the intense and low-energy transition. Nevertheless, the spectra of YR6 and JD10 featured another absorption band that was less intense and more blue-shifted than those mentioned above. The transitions of these bands for JD10 and YR6 involved mixed transitions from low-lying orbitals (e.g., HOMO−1) to higher-energy orbitals (e.g., LUMO+1). Figure S1 displays the HOMO, HOMO−1, LUMO, and LUMO+1 of JD10 and YR6. The electron densities of these four frontier orbitals were not distributed throughout the entire molecular backbones. The electron densities of the HOMOs were distributed mainly

around the electron-donating group, the SQ ring, and the indoline ring; the electron densities of LUMOs were distributed mainly around the R moiety (CPDT in JD10; thiophene in YR6) and the anchoring moiety. These features may have arisen from the twisted geometry between the indoline ring and the R moiety. Therefore, the HOMO to LUMO transitions of JD10 and YR6 were similar to those of the other SQ dyes. Moreover, JD10 and YR6 could undergo an additional transition from low-lying orbitals to high-energy orbitals.

Table 1 lists the optical data of dyes adsorbed on $(\text{TiO}_2)_{38}$ clusters calculated in water, as well as experimental data for these dyes absorbed on TiO_2 thin films. The calculated UV–vis spectra reveal a similar trend with respect to the experimental spectra. The smallest absolute deviation from the experimental values was 6 nm (blue-shifted) for SQ4, while the largest absolute deviation from experiments was 50 nm (blue-shifted) for SQ01. These deviations are also larger than those found for our previously studied organic dyes, W-dyes, that had comparatively small deviations of 1–26 nm in dye– $(\text{TiO}_2)_{38}$

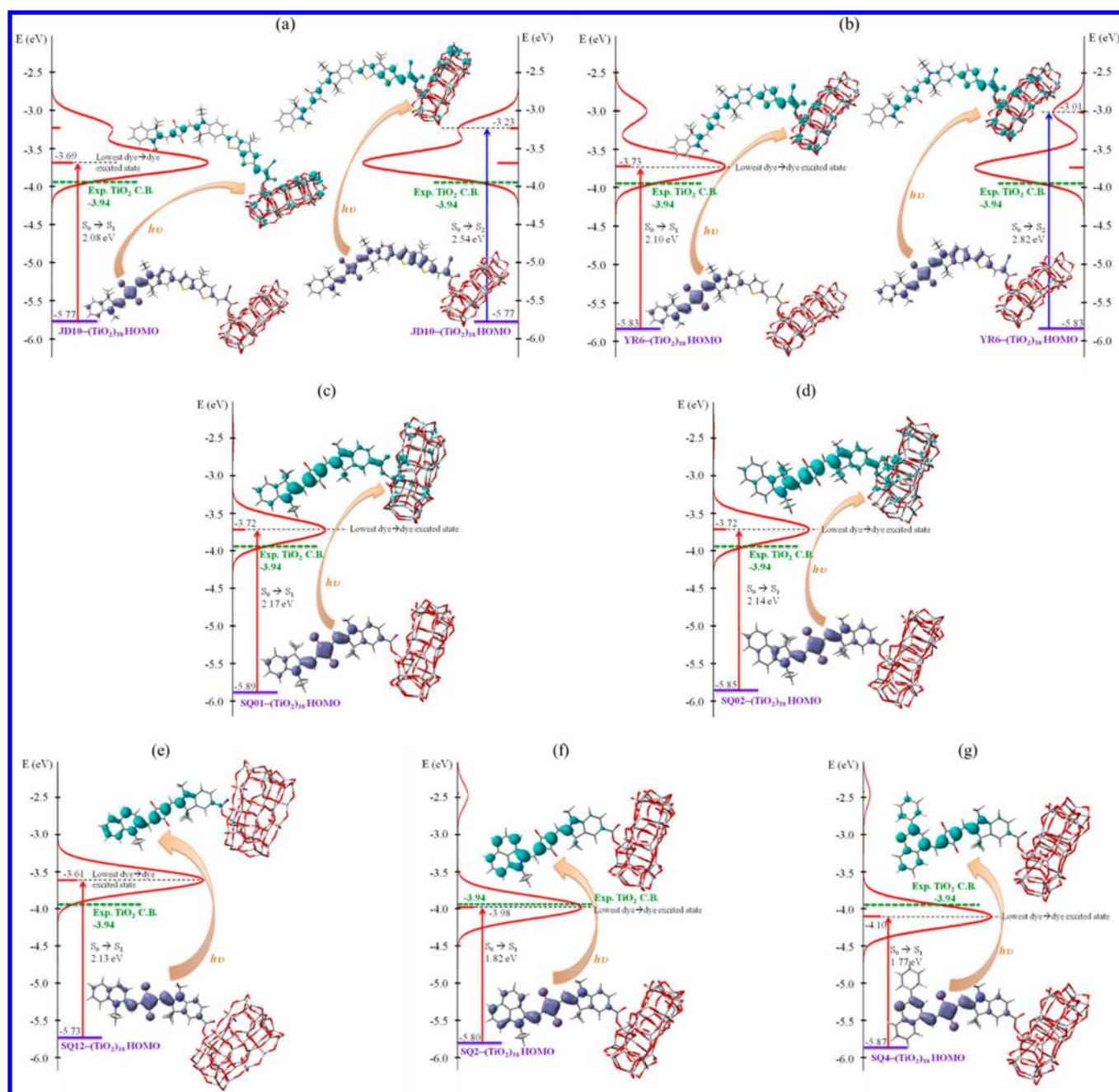


Figure 4. Alignment of the ground and excited state energy levels for the dye–(TiO₂)₃₈ systems and the EDDMs for the dye–(TiO₂)₃₈ systems before (the purple represents where the electron density is coming from) and after (the cyan represents where the electron density is going) photoexcitation. Green dashed and purple solid lines indicate the experimental TiO₂ conduction band (CB) edge and the calculated HOMO energy levels of dye–(TiO₂)₃₈ systems, respectively. (a) JD10–(TiO₂)₃₈, (b) YR6–(TiO₂)₃₈, (c) SQ01–(TiO₂)₃₈, (d) SQ02–(TiO₂)₃₈, (e) SQ12–(TiO₂)₃₈, (f) SQ2–(TiO₂)₃₈, and (g) SQ4–(TiO₂)₃₈ systems.

systems.⁴⁰ Similar to the spectra in solution, our calculations revealed that JD10–(TiO₂)₃₈ and YR6–(TiO₂)₃₈ would provide two intense bands.

Electron Transfer of Dyes upon Photo-Excitation.

Table 3 summarizes the EDDMs of the seven studied SQ dyes at their protonated states in EtOH before (where the electron density is coming from) and after (where the electron density is going) photoexcitation, classified by their various moieties: each dye molecule is partitioned by “donor,” “SQ,” “indoline,” “R,” and “anchor” (from the left side to right side of molecules shown in Figure 3). The “donors” are quinoline for SQ12, benz[*c,d*]indolium for SQ2, benzo-1-thiopyrylium for SQ4, and

indoline ring for others; the “R” groups are only for JD10 and YR6 and are CPDT for JD10 and thiophene for YR6; and the “anchors” are cyanoacrylic acid for JD10 and YR6 and carboxylic acid for other dyes. SQ01, SQ02, SQ12, SQ2, and SQ4 almost have no (or only negligible) electron density transferred to the anchoring groups (carboxylic acid moieties). These results (Table 3) indicate that the electron density of these SQ-derived dye sensitizers in EtOH was not transferred toward the anchoring group upon excitation. More interestingly, the electron density of the quinoline of SQ12 is increased by 20% after excitation indicating that the direction of electron transfer is away from the anchoring group. Mulliken charge

analysis show the quinoline moiety of SQ12 having a net charge of $+0.41e$ is more electropositive than the corresponding moieties of other dyes; for examples, the corresponding indoline moiety (the one away from the anchoring group) of SQ01 has a net charge of $+0.28e$ and the corresponding benzo[e]indole moiety of SQ02 has a net charge of $+0.30e$. These results indicate that the quinoline moiety of SQ12 is more capable to gain more electron density after photoexcitation than the corresponding moieties of other dyes. On the other hand, for the two absorption bands of JD10 and YR6, the electron densities of the anchoring groups increased moderately. These results indicate that, in EtOH, the electron density of JD10 and YR6 is transferred toward the anchoring groups upon excitation.

To investigate the electron transfer upon excitation of the dye molecules adsorbed to TiO_2 , we calculated the UV-vis spectra of dyes adsorbed on a $(\text{TiO}_2)_{38}$ cluster exposing an anatase (101) surface, as a model for the corresponding DSCs. Table 4 lists the calculated orbital contributions of the studied dye- $(\text{TiO}_2)_{38}$ systems upon photoexcitation and their EDDMs before and after photoexcitation. The most-intense, red-shifted transitions of the JD10- $(\text{TiO}_2)_{38}$ and YR6- $(\text{TiO}_2)_{38}$ systems featured electronic transition from the HOMO mainly located on dye to the LUMO mainly located on dye and some higher-energy unoccupied orbitals located on $(\text{TiO}_2)_{38}$; these transitions have the electron density of excited states significantly delocalized into the semiconductors, which received 53 and 45% of the electron density after photoexcitation for the JD10- $(\text{TiO}_2)_{38}$ and YR6- $(\text{TiO}_2)_{38}$ systems, respectively. Parts a and b of Figure 4 display the alignment of energy levels of JD10- $(\text{TiO}_2)_{38}$ and YR6- $(\text{TiO}_2)_{38}$ systems and their electron density difference between ground state and excited state. The energy alignment was calculated by the method first proposed by De Angelis and co-workers,^{66,67} which combines the occupied energy level and the TD-DFT excitations spectra. This method has been employed to align the energy levels of Ru-complexes with complex UV-vis transitions involving higher-energy unoccupied orbitals.⁶⁸ The excited state energy level is accordingly calculated at -3.69 and -3.73 eV for the lower-energy transitions of JD10- $(\text{TiO}_2)_{38}$ and YR6- $(\text{TiO}_2)_{38}$ systems, respectively, with corresponding lowest driving force for excited-state electron injection of ca. 0.21 – 0.25 eV [in relative to the energy level of experimental TiO_2 conduction band (-3.94 eV)]. The less-intense, higher-energy transitions of the JD10- $(\text{TiO}_2)_{38}$ and YR6- $(\text{TiO}_2)_{38}$ systems featured similar orbital contributions as their lower-energy transitions, instead, they involved electronic transition from the HOMO and lower-energy occupied HOMO-1 on dye; these transitions also have the electron density of excited states significantly delocalized into the semiconductors, which received 47 and 51% of the electron density directly after photoexcitation for the JD10- $(\text{TiO}_2)_{38}$ and YR6- $(\text{TiO}_2)_{38}$ systems, respectively. The excited state energy levels of these higher-energy transitions of JD10- $(\text{TiO}_2)_{38}$ and YR6- $(\text{TiO}_2)_{38}$ systems are accordingly calculated at -3.23 and -3.01 eV, respectively, with corresponding the lowest driving force for excited-state electron injection of ca. 0.71 and 0.93 eV, respectively. Considering the strong admixture of dye/semiconductor unoccupied states and the driving force for excited-state electron injection, JD10 and YR6 follow direct electron injection mechanism when excited at their less-intense/high-energy and most-intense/low-energy bands.

SQ01- $(\text{TiO}_2)_{38}$ and SQ02- $(\text{TiO}_2)_{38}$ systems featured electronic transitions mainly from the HOMO located on dye to the LUMO mainly located on dye and partially located on $(\text{TiO}_2)_{38}$; these transitions have the electron density of excited states partially delocalized into the semiconductors, which received ca. 20% of the electron density after photoexcitation. The calculated excited state energy levels (-3.72 eV) of SQ01- $(\text{TiO}_2)_{38}$ and SQ02- $(\text{TiO}_2)_{38}$ systems (Figure 4, parts c and d) are the same and are similar to those of the most-intense/low-energy bands of JD10- $(\text{TiO}_2)_{38}$ and YR6- $(\text{TiO}_2)_{38}$ systems; the corresponding lowest driving force of SQ01- $(\text{TiO}_2)_{38}$ and SQ02- $(\text{TiO}_2)_{38}$ systems for electron injection is ca. 0.22 eV. Interestingly, the $(\text{TiO}_2)_{38}$ moieties in the SQ01- $(\text{TiO}_2)_{38}$ and SQ02- $(\text{TiO}_2)_{38}$ systems received 21 and 20%, respectively, of the electron density after photoexcitation. In the EtOH solutions, our calculations revealed that negligible electron density transferred from SQ01 or SQ02 to the anchoring groups, suggesting that SQ01 and SQ02 might have good orbital match with the $(\text{TiO}_2)_{38}$ cluster.

On the other hand, SQ12- $(\text{TiO}_2)_{38}$, SQ2- $(\text{TiO}_2)_{38}$, and SQ4- $(\text{TiO}_2)_{38}$ systems featured electronic transitions mainly from the HOMO located on dye to the LUMO located on dye; the electron density was redistributed mainly between the donor, SQ, and indoline moieties after excitation. Thus, for the transitions of SQ12- $(\text{TiO}_2)_{38}$, SQ2- $(\text{TiO}_2)_{38}$, and SQ4- $(\text{TiO}_2)_{38}$ systems, almost no or negligible electron density was transferred to the anchor moiety or to the $(\text{TiO}_2)_{38}$ moiety upon excitation. In contrast to other studied SQ dyes, the calculated excited state energy levels of SQ2- $(\text{TiO}_2)_{38}$ and SQ4- $(\text{TiO}_2)_{38}$ systems (Figure 4, parts f and g) are -3.98 and -4.10 eV, respectively, which are slightly lower than the energy level of experimental TiO_2 conduction band (-3.94 eV), providing no additional driving force for excited-state electron injection. Therefore, SQ2 and SQ4 follow indirect electron injection mechanism upon excitation. The SQ12- $(\text{TiO}_2)_{38}$ system has the highest excited state energy level (-3.61 eV) than others giving the lowest driving force for excited-state electron injection of ca. 0.33 eV (Figure 4e); however, the SQ12- $(\text{TiO}_2)_{38}$ system has only negligible electron density transferred to the $(\text{TiO}_2)_{38}$ upon excitation indicating the weak coupling between SQ12 and $(\text{TiO}_2)_{38}$. Thus, SQ12 follows indirect electron injection mechanism upon excitation.

A previous study using a periodic TiO_2 slab exposing anatase (101) surfaces concluded that both direct and indirect charge injection mechanisms are active in the SQ system.³⁷ In the direct electron injection mechanism, electrons are injected to the TiO_2 directly upon excitation; here, the excited state of the dye sensitizer can be described as an oxidized state, while TiO_2 can be considered as being in a reduced state.⁶⁹ On the other hand, the indirect electron injection mechanism is a multistep process involving several steps of electron transfer to the appropriate band of a semiconductor. Therefore, the direct mechanism should give rise to more efficient electron injection to TiO_2 .

A very low or negligible proportion of electron density injected into TiO_2 and/or no driving force for excited-state electron injection suggests that such a dye would not generate a device exhibiting an efficient value of J_{sc} . Accordingly, we suspected that the dyes SQ12, SQ2, and SQ4 would be unlikely to generate high values of J_{sc} . SQ2 and SQ4 have their excited energy levels lower in energy than the $(\text{TiO}_2)_{38}$ conduction band edge, which has no additional driving force for excited-state electron injection; in addition, upon excitation

SQ2 and SQ4 have only negligible proportion of electron density transferred into TiO_2 . Although SQ12 has a higher driving force for excited-state electron injection, the excited electron was transferred mainly toward the donating group that retarded its electron injection into the TiO_2 moiety. Experimental measurements (Table S1, Supporting Information) agree with our calculations, revealing that the values of J_{sc} for devices based on SQ12, SQ2, and SQ4 were significantly lower ($<7 \text{ mA cm}^{-2}$) than those based on our other studied SQ dyes ($>10 \text{ mA cm}^{-2}$).

On the other hand, our calculations reveal that SQ01, SQ02, JD10, and YR6 all have similar lowest driving force for excited-state electron injection of ca. 0.2 eV. SQ01 and SQ02 have electron density partially injected into the TiO_2 moiety (ca. 20%) upon excitation suggesting that these dyes would likely generate devices exhibiting moderate values of J_{sc} . Indeed, experimental measurements revealed that devices based on SQ01 and SQ02 had values of J_{sc} greater than 10 mA cm^{-2} . Using Green's function, Jones and Troisi demonstrated that if the LUMO of a dye has only a small proportion of the electron density distributed at the anchoring group, its rate of reaction will decrease.⁸ Interestingly, although SQ12 has a higher-energy excited state, its proportion of electron density transfer to TiO_2 was also 5%. Our EDDM analysis of SQ12 in EtOH revealed that its electron transfer occurred toward the donating group that retarded electron transfer to the TiO_2 side. Transient absorption spectroscopy⁷⁰ of SQ12 and SQ8 (analogous to SQ01 studied here)⁷¹ has revealed that the rate constant for electron injection (k_{ei}) of SQ12 in iodide electrolyte ($k_{\text{ei}} = 6.9 \times 10^{-10} \text{ s}^{-1}$) is approximately two times smaller than that of SQ8 ($k_{\text{ei}} = 13.2 \times 10^{-10} \text{ s}^{-1}$). These results agree with our calculations: upon photoexcitation, the proportion of electron density transferred to TiO_2 from SQ01 (an analogue of SQ8) was larger than that transferred from SQ12.

JD10 and YR6 have an additional higher-energy/less intense band than others; both transitions have significant proportions of electron density injected into the TiO_2 moiety upon excitation, suggesting that these dyes would likely generate devices exhibiting higher values of J_{sc} . Indeed, experimental measurements revealed that devices based on JD10 and YR6 had values of J_{sc} up to 16.4 and 14.8 mA cm^{-2} , respectively, which are higher than those of other studied SQ dyes. The calculated probabilities of electron density being injected into TiO_2 as well as the lowest driving force for excited-state electron injection from these studied SQ dyes are compatible with their experimentally observed values of J_{sc} . We note that values of J_{sc} are not determined solely by the proportion of electron density injected into TiO_2 upon excitation; other loss mechanisms (e.g., charge recombination) must also be considered in the electron injection mechanism, but such a study is outside the scope of this present investigation.

CONCLUSION

We have employed DFT and TD-DFT to investigate the structural, optical, and electron transfer properties of seven recently published SQ-derived dyes in solution and adsorbed on a $(\text{TiO}_2)_{38}$ cluster. The $(\text{TiO}_2)_{38}$ cluster has an anatase (101) surface; we used the dye- $(\text{TiO}_2)_{38}$ systems as models of corresponding DSCs. When these dyes were adsorbed on $(\text{TiO}_2)_{38}$, upon excitation they followed different direct and indirect mechanisms of electron injection to TiO_2 depending on the localization of the excited state electron density and the lowest driving force for excited-state electron injection.

JD10 and YR6 have two transitions, which follow direct mechanism of electron injection; both of their transitions have significant proportions of electron density delocalized into the TiO_2 moiety upon excitation ($>45\%$) and have the driving forces for excited-state electron injection. JD10 and YR6 based devices indeed generate higher values of J_{sc} than those of other studied dyes. In contrast, electron injection from SQ12, SQ2, and SQ4 dyes upon excitation followed the indirect electron injection mechanism; these dyes have very low or negligible proportion of electron density injected into TiO_2 ($\leq 5\%$). In addition, SQ2 and SQ4 have no additional driving force for excited-state electron injection. SQ12, SQ2, and SQ4 based devices actually have the lowest values of J_{sc} than those of other studied dyes. SQ01 and SQ02 have similar lowest driving forces as those of JD10 and YR6; however, SQ01 and SQ02 have smaller electron density delocalized into the TiO_2 moiety (ca. 20%) upon excitation than those of JD10 and YR6. Experiments show SQ01 and SQ02 based devices generate J_{sc} values lower than those of JD10 and YR6 and are higher than those of SQ12, SQ2, and SQ4. The calculated probabilities of electron density being delocalized into TiO_2 and the calculated driving force for excited-state electron injection from these studied SQ dyes are compatible with their experimentally observed values of J_{sc} . Our study provides insight into the electron transfer mechanisms of SQ-derived dyes adsorbed on TiO_2 upon photoexcitation.

ASSOCIATED CONTENT

Supporting Information

Selected frontier MOs of SQ01, JD10, and YR6 at their protonated states in EtOH, detailed photovoltaic parameters of studied SQ dye sensitized solar cells, and detailed references 2, 11, 13, 16, and 45. This material is available free of charge via the Internet at <http://pubs.acs.org>.

AUTHOR INFORMATION

Corresponding Author

*(H.-H.G.T.) hhtsai@cc.ncu.edu.tw. Telephone: +886-3-4227151 ext. 65909.

Notes

The authors declare no competing financial interest.

ACKNOWLEDGMENTS

We thank the Ministry of Science and Technology of Taiwan (Grant No. NSC 102-2113-M-008-008-MY2) for financial support and the National Center for High-Performance Computing and the V'ger computer cluster at the National Central University of Taiwan for allowing access to computer time and facilities.

REFERENCES

- (1) O'Regan Brian, G. M. A Low-Cost, High-Efficiency Solar Cell Based on Dye-Sensitized Colloidal TiO_2 Films. *Nature* **1991**, 353, 737–740.
- (2) Péchy, P.; Renouard, T.; Zakeeruddin, S. M.; Humphry-Baker, R.; Comte, P.; Liska, P.; Cevey, L.; Costa, E.; Shklover, V.; Spiccia, L.; et al. Engineering of Efficient Panchromatic Sensitizers for Nanocrystalline TiO_2 -Based Solar Cells. *J. Am. Chem. Soc.* **2001**, 123, 1613–1624.
- (3) Mishra, A.; Fischer, M. K. R.; Bauerle, P. Metal-Free Organic Dyes for Dye-Sensitized Solar Cells: From Structure: Property Relationships to Design Rules. *Angew. Chem., Int. Ed.* **2009**, 48, 2474–2499.

- (4) Yum, J. H.; Baranoff, E.; Wenger, S.; Nazeeruddin, M. K.; Grätzel, M. Panchromatic Engineering for Dye-Sensitized Solar Cells. *Energy Environ. Sci.* **2011**, *4*, 842–857.
- (5) Kim, B. G.; Chung, K.; Kim, J. Molecular Design Principle of All-Organic Dyes for Dye-Sensitized Solar Cells. *Chem.—Eur. J.* **2013**, *19*, 5220–5230.
- (6) Hagfeldt, A.; Boschloo, G.; Sun, L.; Kloo, L.; Pettersson, H. Dye-Sensitized Solar Cells. *Chem. Rev.* **2010**, *110*, 6595–6663.
- (7) Dualeh, A.; Delcamp, J. H.; Nazeeruddin, M. K.; Grätzel, M. Near-Infrared Sensitization of Solid-State Dye-Sensitized Solar Cells with a Squaraine Dye. *Appl. Phys. Lett.* **2012**, *100*, 173512.
- (8) Jones, D. R.; Troisi, A. A Method to Rapidly Predict the Charge Injection Rate in Dye Sensitized Solar Cells. *Phys. Chem. Chem. Phys.* **2010**, *12*, 4625–4634.
- (9) Asbury, J. B.; Anderson, N. A.; Hao, E.; Ai, X.; Lian, T. Parameters Affecting Electron Injection Dynamics from Ruthenium Dyes to Titanium Dioxide Nanocrystalline Thin Film. *J. Phys. Chem. B* **2003**, *107*, 7376–7386.
- (10) Goh, G. K. L.; Le, H. Q.; Huang, T. J.; Hui, B. T. T. Low Temperature Grown ZnO@TiO₂ Core Shell Nanorod Arrays for Dye Sensitized Solar Cell Application. *J. Solid State Chem.* **2014**, *214*, 17–23.
- (11) Chen, C.-Y.; Wang, M.; Li, J.-Y.; Pootrakulchote, N.; Alibabaei, L.; Ngoc-le, C.-h.; Decoppet, J.-D.; Tsai, J.-H.; Grätzel, C.; Wu, C.-G.; et al. Highly Efficient Light-Harvesting Ruthenium Sensitizer for Thin-Film Dye-Sensitized Solar Cells. *ACS Nano* **2009**, *3*, 3103–3109.
- (12) Paek, S.; Choi, H.; Kim, C.; Cho, N.; So, S.; Song, K.; Nazeeruddin, M. K.; Ko, J. Efficient and Stable Panchromatic Squaraine Dyes for Dye-Sensitized Solar Cells. *Chem. Commun.* **2011**, *47*, 2874–2876.
- (13) Kimura, M.; Masuo, J.; Tohata, Y.; Obuchi, K.; Masaki, N.; Murakami, T. N.; Koumura, N.; Hara, K.; Fukui, A.; Yamanaka, R.; et al. Improvement of TiO₂/Dye/Electrolyte Interface Conditions by Positional Change of Alkyl Chains in Modified Panchromatic Ru Complex Dyes. *Chem.—Eur. J.* **2013**, *19*, 1028–1034.
- (14) Yella, A.; Lee, H.-W.; Tsao, H. N.; Yi, C.; Chandiran, A. K.; Nazeeruddin, M. K.; Diau, E. W.-G.; Yeh, C.-Y.; Zakeeruddin, S. M.; Grätzel, M. Porphyrin-Sensitized Solar Cells with Cobalt (II/III)–Based Redox Electrolyte Exceed 12% Efficiency. *Science* **2011**, *334*, 629–634.
- (15) Mathew, S.; Yella, A.; Gao, P.; Humphry-Baker, R.; Curchod, B. F. E.; Ashari-Astani, N.; Tavernelli, I.; Rothlisberger, U.; Nazeeruddin, M. K.; Grätzel, M. Dye-Sensitized Solar Cells with 13% Efficiency Achieved through the Molecular Engineering of Porphyrin Sensitizers. *Nat. Chem.* **2014**, *6*, 242–247.
- (16) Yang, J.; Ganesan, P.; Teuscher, J.; Moehl, T.; Kim, Y. J.; Yi, C.; Comte, P.; Pei, K.; Holcombe, T. W.; Nazeeruddin, M. K.; et al. Influence of the Donor Size in D-Pi-a Organic Dyes for Dye-Sensitized Solar Cells. *J. Am. Chem. Soc.* **2014**, *136*, 5722–5730.
- (17) Chen, G.; Sasabe, H.; Lu, W.; Wang, X.-F.; Kido, J.; Hong, Z.; Yang, Y. J-Aggregation of a Squaraine Dye and Its Application in Organic Photovoltaic Cells. *J. Mater. Chem. C* **2013**, *1*, 6547–6552.
- (18) Chen, G.; Sasabe, H.; Sasaki, Y.; Katagiri, H.; Wang, X.-F.; Sano, T.; Hong, Z.; Yang, Y.; Kido, J. A Series of Squaraine Dyes: Effects of Side Chain and the Number of Hydroxyl Groups on Material Properties and Photovoltaic Performance. *Chem. Mater.* **2014**, *26*, 1356–1364.
- (19) Alex, S.; Santhosh, U.; Das, S. Dye Sensitization of Nanocrystalline TiO₂: Enhanced Efficiency of Unsymmetrical Versus Symmetrical Squaraine Dyes. *J. Photochem. Photobiol., A* **2005**, *172*, 63–71.
- (20) Burke, A.; Schmidt-Mende, L.; Ito, S.; Grätzel, M. A Novel Blue Dye for near-IR ‘Dye-Sensitized’ Solar Cell Applications. *Chem. Commun.* **2007**, 234–236.
- (21) Choi, H.; Kim, J.-J.; Song, K.; Ko, J.; Nazeeruddin, M. K.; Grätzel, M. Molecular Engineering of Panchromatic Unsymmetrical Squaraines for Dye-Sensitized Solar Cell Applications. *J. Mater. Chem.* **2010**, *20*, 3280–3286.
- (22) Hara, K.; Sato, T.; Katoh, R.; Furube, A.; Ohga, Y.; Shinpo, A.; Suga, S.; Sayama, K.; Sugihara, H.; Arakawa, H. Molecular Design of Coumarin Dyes for Efficient Dye-Sensitized Solar Cells. *J. Phys. Chem. B* **2003**, *107*, 597–606.
- (23) Yum, J.-H.; Walter, P.; Huber, S.; Rentsch, D.; Geiger, T.; Nüesch, F.; De Angelis, F.; Grätzel, M.; Nazeeruddin, M. K. Efficient Far Red Sensitization of Nanocrystalline TiO₂ Films by an Unsymmetrical Squaraine Dye. *J. Am. Chem. Soc.* **2007**, *129*, 10320–10321.
- (24) Nazeeruddin, M. K.; Humphry-Baker, R.; Grätzel, M.; Wohrle, D.; Schnurpfeil, G.; Schneider, G.; Hirth, A.; Trombach, N. Efficient near-IR Sensitization of Nanocrystalline TiO₂ Films by Zinc and Aluminum Phthalocyanines. *J. Porphyrins Phthalocyanines* **1999**, *3*, 230–237.
- (25) Qin, C.; Numata, Y.; Zhang, S.; Islam, A.; Yang, X.; Sodeyama, K.; Tateyama, Y.; Han, L. A near-Infrared cis-Configured Squaraine Co-Sensitizer for High-Efficiency Dye-Sensitized Solar Cells. *Adv. Funct. Mater.* **2013**, *23*, 3782–3789.
- (26) Shi, Y.; Hill, R. B.; Yum, J. H.; Dualeh, A.; Barlow, S.; Grätzel, M.; Marder, S. R.; Nazeeruddin, M. K. A High-Efficiency Panchromatic Squaraine Sensitizer for Dye-Sensitized Solar Cells. *Angew. Chem., Int. Ed.* **2011**, *50*, 6619–6621.
- (27) Geiger, T.; Kuster, S.; Yum, J. H.; Moon, S. J.; Nazeeruddin, M. K.; Grätzel, M.; Nüesch, F. Molecular Design of Unsymmetrical Squaraine Dyes for High Efficiency Conversion of Low Energy Photons into Electrons Using TiO₂ Nanocrystalline Films. *Adv. Funct. Mater.* **2009**, *19*, 2720–2727.
- (28) Li, J.-Y.; Chen, C.-Y.; Lee, C.-P.; Chen, S.-C.; Lin, T.-H.; Tsai, H.-H.; Ho, K.-C.; Wu, C.-G. Unsymmetrical Squaraines Incorporating the Thiophene Unit for Panchromatic Dye-Sensitized Solar Cells. *Org. Lett.* **2010**, *12*, 5454–5457.
- (29) Li, J. Y.; Lin, T. H.; Chen, S. C.; Wu, C. G. Unsymmetrical Squaraines Incorporating Cabazole as a Donor for Dye-Sensitized Solar Cells. *J. Chin. Chem. Soc. (Taipei, Taiwan)* **2012**, *59*, 1337–1344.
- (30) Pandey, S. S.; Watanabe, R.; Fujikawa, N.; Shivashimpi, G. M.; Ogomi, Y.; Yamaguchi, Y.; Hayase, S. Effect of Extended Pi-Conjugation on Photovoltaic Performance of Dye Sensitized Solar Cells Based on Unsymmetrical Squaraine Dyes. *Tetrahedron* **2013**, *69*, 2633–2639.
- (31) Sreejith, S.; Carol, P.; Chithra, P.; Ajayaghosh, A. Squaraine Dyes: A Mine of Molecular Materials. *J. Mater. Chem.* **2008**, *18*, 264–274.
- (32) Li, H.-B.; Zhang, J.; Wu, Y.; Jin, J.-L.; Duan, Y.-A.; Su, Z.-M.; Geng, Y. Theoretical Study and Design of Triphenylamine-Malononitrile-Based P-Type Organic Dyes with Different Π -Linkers for Dyes-Sensitized Solar Cells. *Dyes Pigments* **2014**, *108*, 106–114.
- (33) Han, L. H.; Zhang, C. R.; Zhe, J. W.; Jin, N. Z.; Shen, Y. L.; Wang, W.; Gong, J. J.; Chen, Y. H.; Liu, Z. J. Understanding the Electronic Structures and Absorption Properties of Porphyrin Sensitizers Yd₂ and Yd₂-o-C₈ for Dye-Sensitized Solar Cells. *Int. J. Mol. Sci.* **2013**, *14*, 20171–20188.
- (34) El-Shishtawy, R. M.; Asiri, A. M.; Aziz, S. G.; Elroby, S. A. Molecular Design of Donor-Acceptor Dyes for Efficient Dye-Sensitized Solar Cells I: A Dft Study. *J. Mol. Model.* **2014**, *20*, 2241.
- (35) Velusamy, M.; Hsu, Y. C.; Lin, J. T.; Chang, C. W.; Hsu, C. P. 1-Alkyl-1H-imidazole-Based Dipolar Organic Compounds for Dye-Sensitized Solar Cells. *Chem.—Asian J.* **2010**, *5*, 87–96.
- (36) Wu, C.-G.; Chung, M.-F.; Tsai, H.-H. G.; Tan, C.-J.; Chen, S.-C.; Chang, C.-H.; Shih, T.-W. Fluorene-Containing Organic Photosensitizers for Dye-Sensitized Solar Cells. *ChemPlusChem* **2012**, *77*, 832–843.
- (37) Rocca, D.; Gebauer, R.; De Angelis, F.; Nazeeruddin, M. K.; Baroni, S. Time-Dependent Density Functional Theory Study of Squaraine Dye-Sensitized Solar Cells. *Chem. Phys. Lett.* **2009**, *475*, 49–53.
- (38) Zhu, C.; Liang, J.; Cao, Z. Unique Metal Dicarboxylate Dyes with Excellent Photoelectronic Properties for Solar Cells: Insight from Density Functional Calculations. *J. Phys. Chem. C* **2013**, *117*, 13388–13395.

- (39) Liang, J.; Zhu, C.; Cao, Z. Electronic and Optical Properties of the Triphenylamine-Based Organic Dye Sensitized TiO₂ Semiconductor: Insight from First Principles Calculations. *Phys. Chem. Chem. Phys.* **2013**, *15*, 13844–13851.
- (40) Wu, C. G.; Shieh, W. T.; Yang, C. S.; Tan, C. J.; Chang, C. H.; Chen, S. C.; Wu, C. Y.; Tsai, H. H. G. Molecular Engineering of Cyclopentadithiophene-Containing Organic Dyes for Dye-Sensitized Solar Cell: Experimental Results Vs Theoretical Calculation. *Dyes Pigments* **2013**, *99*, 1091–1100.
- (41) Maeda, T.; Shirna, N.; Tsukamoto, T.; Yagi, S.; Nakazumi, H. Unsymmetrical Squarylium Dyes with Pi-Extended Heterocyclic Components and Their Application to Organic Dye-Sensitized Solar Cells. *Synth. Met.* **2011**, *161*, 2481–2487.
- (42) Becke, A. D. Density-Functional Thermochemistry. Iii. The Role of Exact Exchange. *J. Chem. Phys.* **1993**, *98*, 5648.
- (43) Lee, C.; Yang, W.; Parr, R. G. Development of the Colle-Salvetti Correlation-Energy Formula into a Functional of the Electron Density. *Phys. Rev. B* **1988**, *37*, 785.
- (44) Petersson, G. A.; Al-Laham, M. A. A Complete Basis Set Model Chemistry. II. Open-Shell Systems and the Total Energies of the First-Row Atoms. *J. Chem. Phys.* **1991**, *94*, 6081.
- (45) Frisch, M. J.; Trucks, G. W.; Schlegel, H. B.; Scuseria, G. E.; Robb, M. A.; Cheeseman, J. R.; Scalmani, G.; Barone, V.; Mennucci, B.; Petersson, G. A., et al., Gaussian, Inc.: Wallingford CT, 2009.
- (46) Cossi, M.; Rega, N.; Scalmani, G.; Barone, V. Energies, Structures, and Electronic Properties of Molecules in Solution with the C-Pcm Solvation Model. *J. Comput. Chem.* **2003**, *24*, 669–681.
- (47) Yanai, T.; Tew, D. P.; Handy, N. C. A New Hybrid Exchange-Correlation Functional Using the Coulomb-Attenuating Method (Cam-B3lyp). *Chem. Phys. Lett.* **2004**, *393*, 51–57.
- (48) Yakhanthip, T.; Jungsuttiwong, S.; Namuangruk, S.; Kungwan, N.; Promarak, V.; Sudyoasuk, T.; Kochpradist, P. Theoretical Investigation of Novel Carbazole-Fluorene Based D- Π -a Conjugated Organic Dyes as Dye-Sensitizer in Dye-Sensitized Solar Cells (Dscs). *J. Comput. Chem.* **2011**, *32*, 1568–1576.
- (49) Pastore, M.; Angelis, F. D. Aggregation of Organic Dyes on TiO₂ in Dye-Sensitized Solar Cells Models: An Ab Initio Investigation. *ACS Nano* **2010**, *4*, 556–562.
- (50) Chen, P.; Yum, J. H.; Angelis, F. D.; Mosconi, E.; Fantacci, S.; Moon, S.-J.; Baker, R. H.; Ko, J.; Nazeeruddin, M. K.; Grätzel, M. High Open-Circuit Voltage Solid-State Dye-Sensitized Solar Cells with Organic Dye. *Nano Lett.* **2009**, *9*, 2487–2492.
- (51) Delley, B. An All-Electron Numerical Method for Solving the Local Density Functional for Polyatomic Molecules. *J. Chem. Phys.* **1990**, *92*, 508.
- (52) Delley, B. From Molecules to Solids with the Dmol[Sup 3] Approach. *J. Chem. Phys.* **2000**, *113*, 7756.
- (53) Perdew, J. P.; Burke, K.; Ernzerhof, M. Generalized Gradient Approximation Made Simple. *Phys. Rev. Lett.* **1996**, *77*, 3865–3868.
- (54) Perdew, J. P.; Chevary, J. A.; Vosko, S. H.; Jackson, K. A.; Pederson, M. R.; Singh, D. J.; Fiolhais, C. Atoms, Molecules, Solids, and Surfaces: Applications of the Generalized Gradient Approximation for Exchange and Correlation. *Phys. Rev. B: Condens. Matter* **1992**, *46*, 6671–6687.
- (55) O'Boyle, N. M.; Tenderholt, A. L.; Langner, K. M. Cclib: A Library for Package-Independent Computational Chemistry Algorithms. *J. Comput. Chem.* **2008**, *29*, 839–845.
- (56) Paterson, M. J.; Blancafort, L.; Wilsey, S.; Robb, M. A. Photoinduced Electron Transfer in Squaraine Dyes: Sensitization of Large Band Gap Semiconductors. *J. Phys. Chem. A* **2002**, *106*, 11431–11439.
- (57) Yesudas, K.; Chaitanya, G. K.; Prabhakar, C.; Bhanuprakash, K.; Rao, V. J. Structure, Bonding, and Lowest Energy Transitions in Unsymmetrical Squaraines: A Computational Study. *J. Phys. Chem. A* **2006**, *110*, 11717–11729.
- (58) Ning, Z. J.; Fu, Y.; Tian, H. Improvement of Dye-Sensitized Solar Cells: What We Know and What We Need to Know. *Energy Environ. Sci.* **2010**, *3*, 1170–1181.
- (59) Jungsuttiwong, S.; Yakhanthip, T.; Surakhot, Y.; Khunchalee, J.; Sudyoasuk, T.; Promarak, V.; Kungwan, N.; Namuangruk, S. The Effect of Conjugated Spacer on Novel Carbazole Derivatives for Dye-Sensitized Solar Cells: Density Functional Theory/Time-Dependent Density Functional Theory Study. *J. Comput. Chem.* **2012**, *33*, 1517–1523.
- (60) Choi, H.; Lee, J. K.; Song, K.; Kang, S. O.; Ko, J. Novel Organic Dyes Containing Bis-Dimethylfluorenyl Amino Benzo[B]Thiophene for Highly Efficient Dye-Sensitized Solar Cell. *Tetrahedron* **2007**, *63*, 3115–3121.
- (61) Hua, Y.; Chang, S.; Huang, D. D.; Zhou, X.; Zhu, X. J.; Zhao, J. Z.; Chen, T.; Wong, W. Y.; Wong, W. K. Significant Improvement of Dye-Sensitized Solar Cell Performance Using Simple Phenothiazine-Based Dyes. *Chem. Mater.* **2013**, *25*, 2146–2153.
- (62) Srinivas, K.; Prabhakar, C.; Devi, C. L.; Yesudas, K.; Bhanuprakash, K.; Rao, V. J. Enhanced Diradical Nature in Oxyallyl Derivatives Leads to near Infra Red Absorption: A Comparative Study of the Squaraine and Croconate Dyes Using Computational Techniques. *J. Phys. Chem. A* **2007**, *111*, 3378–3386.
- (63) Steiner, E. Density-Difference Maps in Quantum Chemistry. *Theor. Chim. Acta* **1982**, *60*, 561–572.
- (64) Ding, W.-L.; Wang, D.-M.; Geng, Z.-Y.; Zhao, X.-L.; Xu, W.-B. Density Functional Theory Characterization and Verification of High-Performance Indoline Dyes with D-a- Π -a Architecture for Dye-Sensitized Solar Cells. *Dyes Pigments* **2013**, *98*, 125–135.
- (65) Ding, W.-L.; Wang, D.-M.; Geng, Z.-Y.; Zhao, X.-L.; Yan, Y.-F. Molecular Engineering of Indoline-Based D-a- Π -a Organic Sensitizers toward High Efficiency Performance from First-Principles Calculations. *J. Phys. Chem. C* **2013**, *117*, 17382–17398.
- (66) De Angelis, F.; Fantacci, S.; Mosconi, E.; Nazeeruddin, M. K.; Grätzel, M. Absorption Spectra and Excited State Energy Levels of the N719 Dye on TiO₂ in Dye-Sensitized Solar Cell Models. *J. Phys. Chem. C* **2011**, *115*, 8825–8831.
- (67) Pastore, M.; Fantacci, S.; De Angelis, F. Modeling Excited States and Alignment of Energy Levels in Dye-Sensitized Solar Cells: Successes, Failures, and Challenges. *J. Phys. Chem. C* **2013**, *117*, 3685–3700.
- (68) Tateyama, Y.; Sumita, M.; Ootani, Y.; Aikawa, K.; Jono, R.; Han, L. y.; Sodeyama, K. Acetonitrile Solution Effect on Ru N749 Dye Adsorption and Excitation at TiO₂ Anatase Interface. *J. Phys. Chem. C* **2014**, *118*, 16863–16871.
- (69) Persson, P.; Bergström, R.; Lunell, S. Quantum Chemical Study of Photoinjection Processes in Dye-Sensitized TiO₂ Nanoparticles. *J. Phys. Chem. B* **2000**, *104*, 10348–10351.
- (70) Marchena, M. J.; de Miguel, G.; Cohen, B.; Organero, J. A.; Pandey, S.; Hayase, S.; Douhal, A. Real-Time Photodynamics of Squaraine-Based Dye-Sensitized Solar Cells with Iodide and Cobalt Electrolytes. *J. Phys. Chem. C* **2013**, *117*, 11906–11919.
- (71) The SQ8 is the analogous of SQ01 studied here. The difference of SQ8 and SQ01 in chemical structure is the length of alkyl chains at the indoline rings (ethyl chain for SQ8 and octyl chain for SQ01).